CHAPTER III

GROWTH OF QUANTUM NANOSTRUCTURES AND THEIR CHARACTERIZATION METHODS

In the early 1970s, molecular beam epitaxy (MBE) was invented as a equipment for molecular design of material, particularly as a popular technique for growing III-V compound semiconductors. With clean and ultra high vacuum environment, the atomic or molecular beams of the constituent elements are incident upon a heated substrate crystal. MBE provides several benefits, for instance, it can produce high-quality layers with very abrupt interfaces and good control of thickness, doping, and composition, because of the precise control of beam fluxes and growth conditions. In the atomic structure, quantum effect is strongly found because the electron could show their virgin properties. This gives rise to quantum devices which have high efficiency, high speed and high performance. It can be said that MBE structures closely approximate the idealised models used in solid state theory.

The detail of MBE is presented in the beginning of this chapter. Moreover an in-situ reflection high-electron energy diffraction (RHEED) observation, ex-situ atomic force microscopy (AFM), and photoluminescence (PL) spectroscopy are also presented. Finally, the material consideration and the sample preparation are described in the end of this chapter.

3.1 Molecular beam epitaxy (MBE)

In this research, a modified RIBER 32P MBE machine consisting of three UHV chambers, i.e., introduction chamber, transfer chamber, and growth chamber, is used to grow our samples. Three chambers are separated by isolation gate valves. Pumping system including sorption pump, ion pump, and titanium sublimation pump is installed to keep UHV condition. A figure of RIBER 32P MBE is shown in Figure 3.1. The pressure of each chamber is measured by ionisation gauge. In case of growth chamber, there are two ionisation gauges, one, located at equivalent substrate position behind the substrate heater, is used for beam flux measurement and the other, installed in front of the ion pump, is for background pressure measurement. The substrate is rotated continuously while the epitaxial growth to provide uniform flux profile on substrate surface. The group III and group V elements; In, Ga, Al, and As_4, are contained in pyrolytic boron nitride (PBN) crucibles, installed in separated effusion cells. Each cell is heated by heater which temperature is controlled by feedback from standard

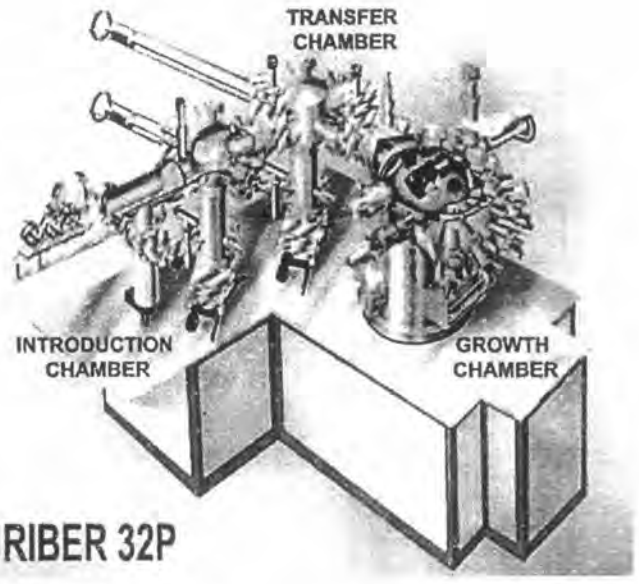

Figure 3.1: The modified RIBER 32P MBE consists of three chambers, i.e., introduction chamber, transfer chamber, and growth chamber.

thermocouple via computer. The beam flux is controlled by tantalum shutter in front of each cell. A schematic drawing of the modified III-V MBE growth chamber is shown in Figure 3.2.

In sample preparation, the substrates need to be preheated, heat treatment process, by heaters in introduction chamber. This is the important process for MBE growth. A propose of preheat process is to eliminated contaminated substance, mainly water (H_2O), on substrate surface. After preheat process, the sample is transferred to the manipulator in growth chamber.

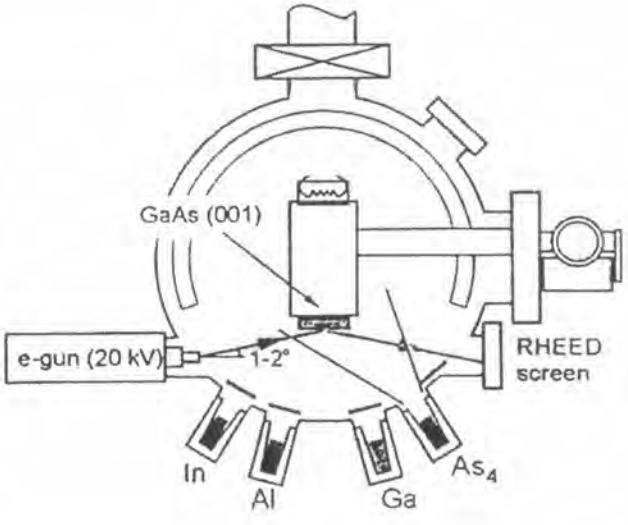

Figure 3.2: Schematic drawing of the modified III-V MBE growth chamber. The chamber is cooled by a closed circuit liquid N_2. The base pressure is less than $1x10^{-10}$ torr.

The unique advantage of MBE from other techniques is that it enables to study and control the growth process in situ. In particular, reflection high energy electron diffraction (RHEED) allows direct measurement of surface structure of the substrate wafer and the already grown epilayer. The equipment of RHEED consists of a 20-kV electron gun, a fluorescent screen, a CCD camera, and a computer. In addition to RHEED, the quadruple mass spectroscopy is installed for particle analysis in growth chamber.

3.2 Reflection high energy electron diffraction (RHEED)

Reflection high energy electron diffraction is an in-situ tool for characterising thin films. It allows direct measurements of the surface structure of the substrate wafer and already grown epilayer. It also allows observation of the dynamics of MBE growth. The schematic diagram of RHEED setup is shown in Figure 3.3. An accelerated electron beam ($\backsim$15 keV) is incident on the surface with a glancing angle ($< 3°$) and is reflected. The high energy of the electrons would result in high penetration depth. The scattering electrons interfere constructively and form a pattern on the RHEED screen. The RHEED pattern can be captured with a high-performance CCD camera and analysed with the sophisticated RHEED data processing software.

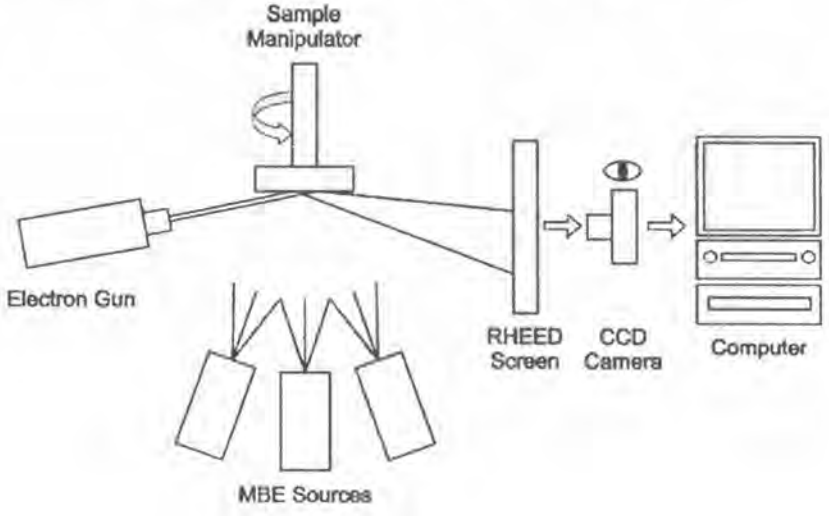

Figure 3.3: Schematic diagram of RHEED setup consisting of electron gun, RHEED screen, high-performance CCD camera and analysed with the sophisticated RHEED data processing software via computer.

3.2.1 RHEED pattern observation

The diffraction of the incoming primary beam leads to the appearance of intensity-modulated streaks (or rods). The experimental geometry of RHEED is illustrated in Figure 3.4 (a) and (b). The short de Broglie wavelength of electron allows a shallow

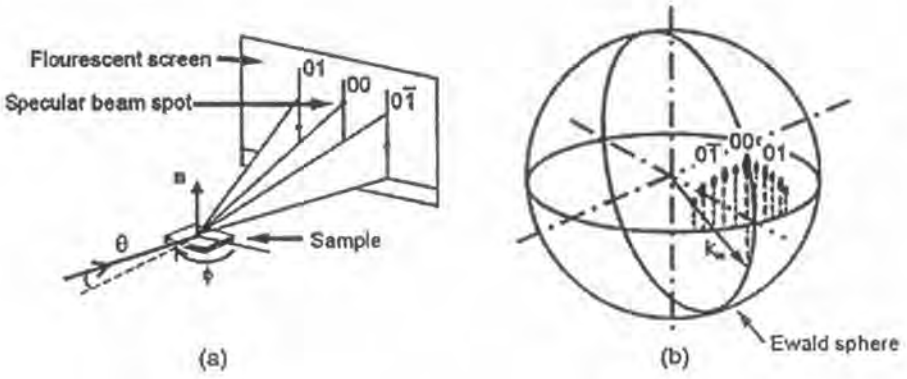

Figure 3.4: (a) Schematic diagram of RHEED geometry showing the incident beam at an angle θ to the surface plane. The elongated spots indicate the intersection of the Ewald sphere with 01, 00, 0$\bar{1}$ rods. (b) Ewald sphere construction for the GaAs (001)-(2x4) reconstructed surface in [$\bar{1}$10] azimuth, illustrating the arc of the short streaks corresponding to the intersection of the sphere with the 01, 00, 0$\bar{1}$ rods [26].

penetration depth into the substrate; therefore, the diffraction pattern is restricted to the very uppermost layers resulting in a Laue condition represented by the reciprocal lattice space rods perpendicular to the real surface [17].

3.2.2 Temperature calibration

Due to the temperature read from thermocouple is not reliable, the transition of the reconstruction pattern as a function of substrate temperature, a calibration method to find the absolute temperature of substrate surface, is investigated. In this work, the (001)-GaAs substrate temperature was decreased with 10°C/min. The RHEED pattern would change from (2x4) to c(4x4) as shown in Figure 3.5. Afterwards, the substrate temperature was increased resulting in RHEED patterns reconstruction from c(4x4) to (2x4). The average temperature of T1, T2, T3 and T4 is defined as 500°C. This transition process is observed under As-rich atmosphere of 6-8x10^{-6} torr.

3.2.3 RHEED Intensity Oscillation

RHEED intensity oscillation is used for measuring growth rates. This has been used to calibrate beam fluxes and control alloy composition and the thickness of the quantum structures [17]. Figure 3.6 illustrates how the oscillations in the intensity of the specular beam occur. There is a maximum reflectivity for the initial and final smooth surface and a minimum for the intermediate state when the growing layer is approximately half complete. Due to the period of oscillation signal, the growth rate of GaAs can be calibrated. The experimental data is shown in Figure 3.7 (a).

On the other hand, in case of InAs growth rate calibration, we use QD formation time of InAs on GaAs substrate, which is a lattice mismatch system. When shutter of In is opened, the RHEED pattern will transform from streaky to spotty pattern during

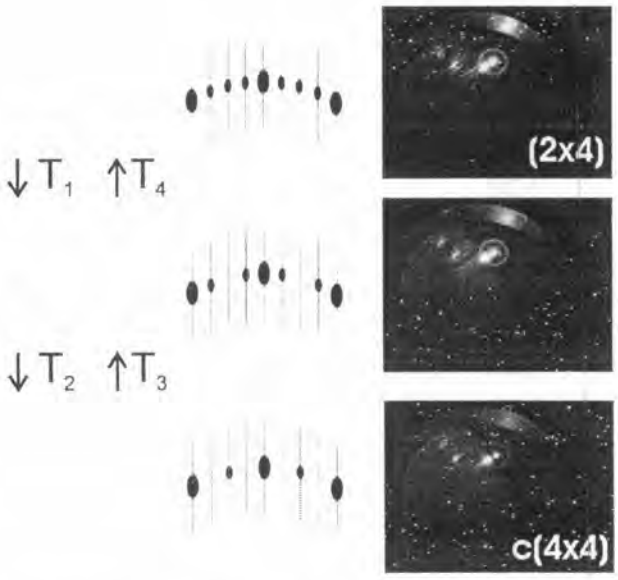

Figure 3.5: Schematic diagram of RHEED pattern transition in [$\bar{1}$10] azimuth of (001) GaAs substrate. The (001) GaAs substrate temperature was decreased and increased with 10 °C/min. The average temperature of T1, T2, T3 and T4 is defined as 500 °C [27].

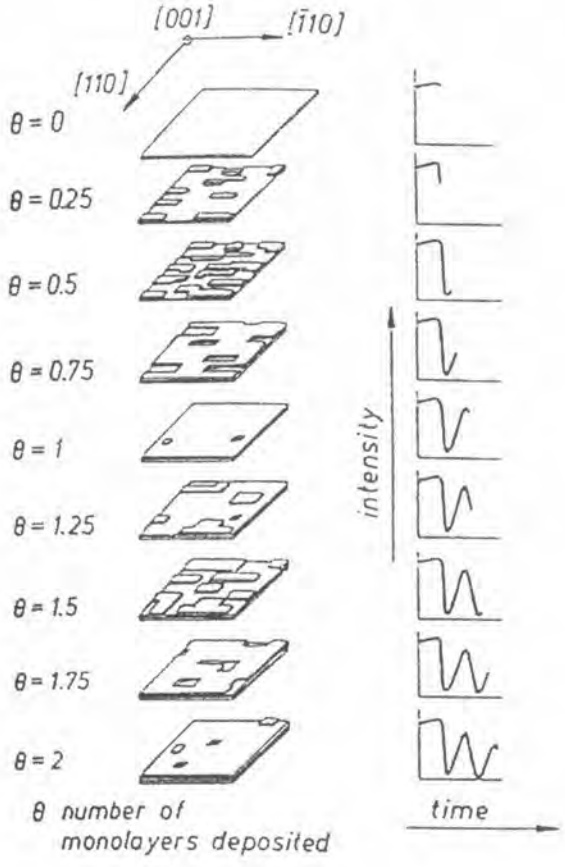

Figure 3.6: Formation of the first two complete monolayer of GaAs (001) related to RHEED intensity oscillations [17].

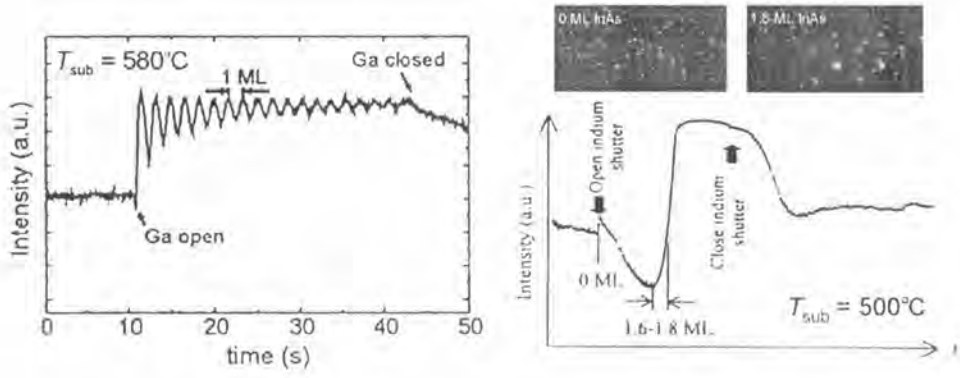

Figure 3.7: RHEED intensity oscillation obtained during the growth of (a) GaAs and the intensity of RHEED oscillation and RHEED patterns of (b) InAs in case of 0 ML and 1.8 ML [26].

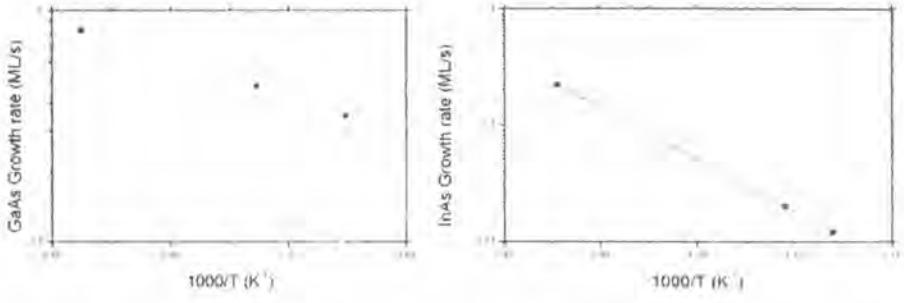

Figure 3.8: Plots of growth rates of GaAs, and InAs as a function of cell temperatures under As-rich condition.

the change of InAs from 2D island to 3D island, which can be defined as about 1.7 ML InAs deposition. The intensity of RHEED oscillation in case of InAs was shown in Figure 3.7 (b). The experimental growth rate of GaAs, AlAs and InAs as a function of cell temperatures is plotted and is shown in Figure 3.8.

3.3 Atomic Force Microscopy (AFM)

The atomic force microscope (AFM) is a very powerful microscope invented by Binnig, Quate and Gerber in 1986. The AFM consists of a cantilever with a sharp tip at its end, typically composed of silicon or silicon nitride with tip sizes on the order of nanometers. The tip is brought into close proximity of a sample surface. Typically, the deflection is measured using a laser spot reflected from the top of the cantilever into an array of photodiodes. The block diagram of AFM is shown in Figure 3.9.

In this work, the AFM images are performed by using SEIKO SPA 400-AFM. The scan rate is about 1-2 Hz and scan size is usually 2x2 μm^2 with 512 data points per scan line. So the lateral resolution is approximately 4 nm (2000 nm/512 data points). Because of the tip convolution, the exact shape and lateral size of the QD structure

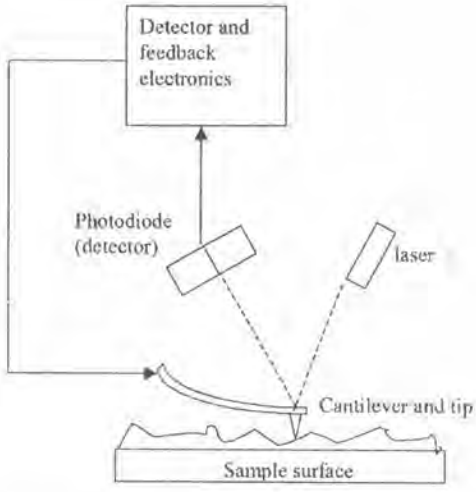

Figure 3.9: Schematic drawing of Atomic Force Microscopy (Drawn October 12, 2002 by Allen Timothy Chang)

may not be correctly determined by this measurement. However, the vertical resolution of this measurement is usually in subnanometer range. Therefore, we use the height distribution of the QD arrays obtained from analysis of the AFM images to determine the size homogeneity of QDs.

3.4 Photoluminescence (PL) spectroscopy

Photoluminescence (PL) spectroscopy is a key system for sample characterisation. The samples with InAs QDs buried in GaAs were excited by the 488-nm line of an Ar+ laser. A block diagram of the PL experimental setup is shown in Figure 3.10. The laser beam was chopped focused to the sample by focal lens. The light signal is analysed by monochrometor. A high-pass filter is used to filter the visible-light noise and the reflected laser beam signal. Then, the resolved light is detected by a InGaAs detector. A chopper and the lock-in amplifier are used to enhance the signal by the standard lock-in technique.

In this work, the interpretation of PL data can simply be described. The ground state PL peak energy contains information about the size of QD, which are described in Figure 3.11. The increasing of QD size results in a lower number of quantized energy levels, which leads to a lower PL peak position. Therefore, this PL peak position can be used to determine the size of QD structure. Moreover, we can investigate the QD size fluctuation from the broadening of PL spectrum described in Figure 3.12, which is measured in terms of full width half maximum (FWHM). In case of single QD, the PL line width is in accordance with delta-like density of state. On the other hand, in case of self-assembled QDs, a large number of QDs with different size result in board PL spectrum. Consequently, we use the PL line width to measure the homogeneity of self-assembled QDs.

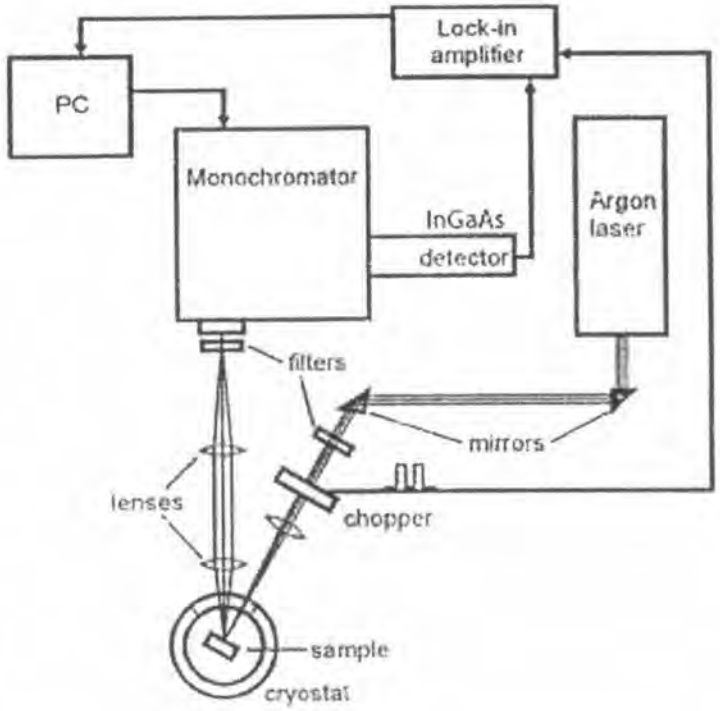

Figure 3.10: Schematic of the PL experimental setup [26].

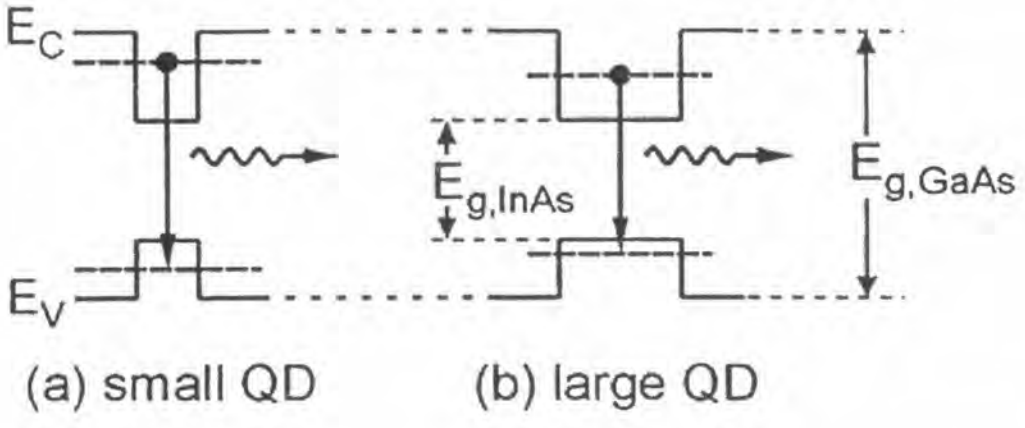

Figure 3.11: PL peak energy contains information about the size of QD. PL peak position of small QD (a) is higher compared with large QD (b) [26].

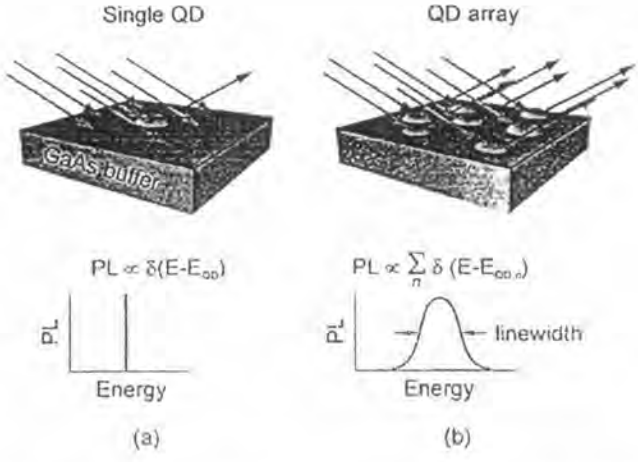

Figure 3.12: (a) The PL spectrum is delta-like function due to single QD. (b) The PL peak position corresponds to the average dot size and the PL line width corresponds to the size distribution of QDs [26].

3.5 Material consideration

The mismatch system between GaAs and InAs play a significant role in many researches. The plot of energy gap versus lattice constant is shown in Figure 3.13. Gallium Arsenide (GaAs) is the chemical compound of gallium and arsenic. Its melting point is 1237 °C. It is an important semiconductor which is used as the base material for high frequency applications such as infrared light-emitting diodes and laser diodes. GaAs devices have several advantages which are superior to silicon devices because GaAs has a higher saturated electron velocity and higher electron mobility, allowing it to operate at high frequencies in excess of 250 GHz. In addition, GaAs devices generate less noise than silicon devices when operated at high frequencies. Moreover, they can also be operated at higher power levels than the equivalent silicon device resulting from their higher breakdown voltages. Furthermore, GaAs has a direct bandgap, which can be used to emit light, while silicon has an indirect bandgap which very poor to emit light. In this work, GaAs-(001) substrates were used due to their cost and their advantages of manufacturing.

Indium arsenide (InAs) is a semiconductor composed of indium and arsenic. Its melting point is about 942 °C. During the past few decades, many proposed that quantum dots, a three-dimensional confinement structure, can be formed in a monolayer of InAs on GaAs. The mismatch of lattice constants between GaAs and InAs is 7 %. This mismatch creates tensions in the surface layer, which leads to formation of the QDs. The general properties and elastic constants of GaAs and InAs are introduced in Table 3.1 and 3.2, respectively.

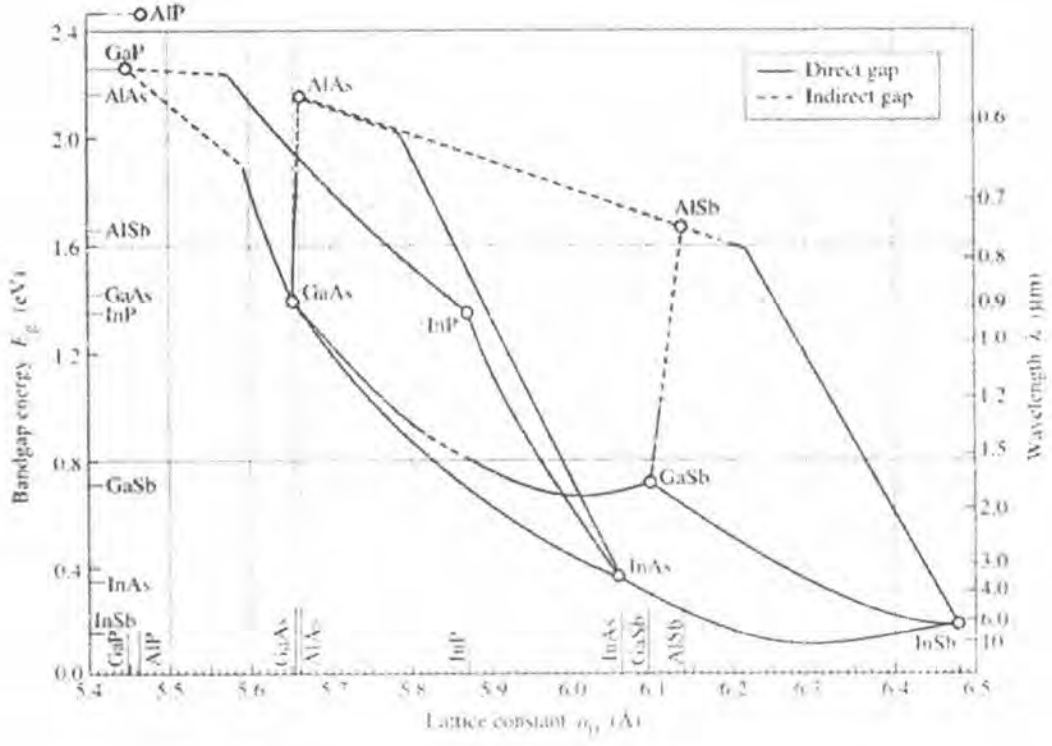

Figure 3.13: Energy bandgap versus lattice constant for common elemental and compound semiconductors. The lines represent the relationship between energy gap of alloy of two binary compounds and lattice constant. The solid line is for direct band gap material and the dotted line is for indirect band gap material [33].

Table 3.1: Properties of GaAs and InAs semiconductors at room temperature (300 K). Direct band is indicated by (D) in the energy gap column adapted from [23].

Parameter	GaAs	InAs
Crystal structure	Zinc blende	Zinc blende
Band gap at 300 K	1.424 eV (D)	0.36 eV (D)
Lattice constant	5.65315 Å	6.05838 Å
Distance between nearest neighbors ($a\sqrt{3/4}$)	2.448 Å	2.623 Å
Melting point	1237 °C	942 °C
Electron effective mass	0.067	0.028
Heavy hole effective mass	0.45	0.33
Electron mobility at 300 K	9200 $cm^2/(V \cdot s)$	22600 $cm^2/(V \cdot s)$
Hole mobility at 300 K	400 $cm^2/(V \cdot s)$	200 $cm^2/(V \cdot s)$

Table 3.2: Elastic constants of GaAs and InAs (10^{11} Pa) [24].

	C_{11}	C_{12}	C_{22}	C_{an}
GaAs	1.18	0.54	0.59	-0.54
InAs	0.83	0.45	0.40	-0.42

3.6 Sample preparation

Epi-ready (001)-GaAs substrates were used as the starting material in all our growths. After deoxidation process, a 300-nm GaAs buffer layer was grown at 580 °C, and then, the investigated structure was grown on the surface after the substrate temperature was decreased to 500 °C. The structure was covered by 100-nm GaAs as a confinement layer at 500 °C for photoluminescence (PL) measurement. Afterwards, the same structure was regrown on the topmost of the surface, and then, the substrate temperature was decreased immediately for AFM measurement. The schematic of sample structure was illustrated in Figure 3.14.

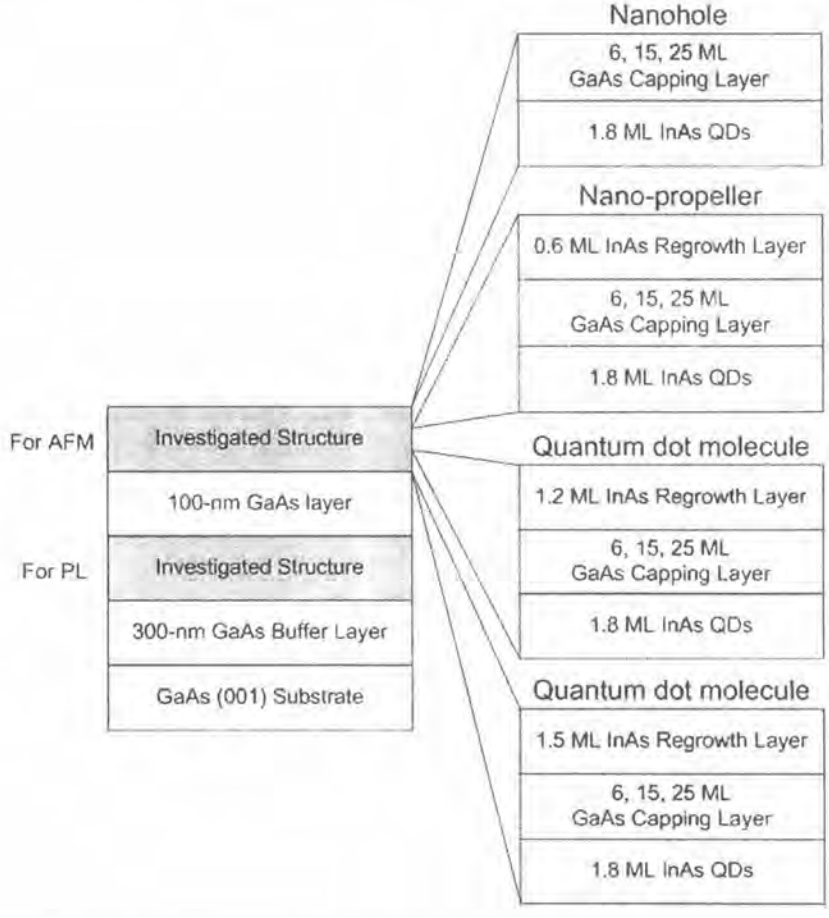

Figure 3.14: Schematic of sample structure and substrate temperature